Characteristics of Radiation Absorption in Metallic Particles

T. Q. Qiu

J. P. Longtin

C. L. Tien

Department of Mechanical Engineering,
University of California,
Berkeley, CA 94720

Thermal radiation absorption in metallic particles is an important phenomenon in many contemporary laser-processing techniques, including laser cladding of coating materials and laser cleaning of particulate contaminations. In this work, the Drude free-electron theory and electromagnetic wave theory are utilized to characterize the internal absorption of CO_2 laser radiation in aluminum, chromium, and nickel particles. The results show that metallic particles have unique radiation properties. Radiation absorption in large particles occurs only in a very narrow region of the front particle surface, which results in inefficient radiation absorption. On the other hand, micron and submicron particles can absorb radiation very efficiently, due to the strong diffraction effect at the particle surface. For extremely small particles (e.g., nanometer particles), radiation absorption becomes less efficient. The particle absorption efficiency is found to increase with temperature, and this temperature dependence can be determined from those of flat metal surfaces at the normal incidence.

Introduction

Laser cladding is a very promising surface modification technique that can dramatically increase surface hardness and surface resistance to wear and corrosion (Komvopoulos and Nagarathnam, 1990; Mazumder et al., 1992). It employs a high-power laser beam to fuse metallic cladding powders to a substrate surface forming a thin layer of novel material. If the cladding powder is well heated before it reaches the cladding surface, less laser energy is required to melt the cladding surface, which in turn improves the cladding quality (Atamert and Bhadeshia, 1989; Oberlander and Lugscheider, 1992) as well as the cladding speed. However, due to the lack of engineering information regarding radiation absorption in the cladding particles, accurate prediction and control of the particle temperature have been difficult (Hoadley and Rappaz, 1992; Pustovalov and Bobuchenko, 1993). The purpose of the present work is to characterize absorption of CO_2 laser radiation at the wavelength of 10.6 μm in aluminum, chromium, and nickel powders.

Radiation-particle interactions often involve strong refraction and diffraction phenomena at the particle surface, which can enhance radiation absorption. Tuntomo et al. (1991) showed that weakly reflecting and absorbing particles absorb radiation most efficiently in certain size regions. For metallic powders, due to their highly conducting nature, a very different size region for efficient radiation absorption is expected. Absorptivity of flat metal surfaces generally increases with temperature for infrared radiation (Prokhorov and Konov, 1990). The temperature dependence of radiation absorption in metallic particles, however, has not been studied. This work utilizes Drude's free-electron theory and classical electromagnetic wave theory to characterize radiation absorption in metallic cladding particles and its temperature dependence.

Analysis

Aluminum, chromium, and nickel powders are commonly used as cladding materials, with the particle diameter ranging from 1 μm to about 100 μm. The powders are delivered into the cladding zone with the assistance of an argon gas flow at a typical particle density around 10^4 cm^{-3} (Komvopoulos and Nagarathnam, 1990; Pustovalov and Bobuchenko, 1993). The distance between individual particles is much larger than the CO_2 laser wavelength (10.6 μm); thus each particle interacts with the laser beam independently (Brewster and Tien, 1982). Multiple radiation scattering by the particles can be well accounted for by the radiation transfer equation once the radiation properties of individual particles are known (Brewster, 1992). Therefore, this study focuses on radiation properties of single particles.

The shape of cladding particles depends strongly on the powder production method and the powder material (Avner, 1964; Hausner and Mal, 1982). For example, powder particles prepared from atomization of liquid metals are typically spherical, while those particles produced from reduction of metal oxides often have irregular shapes, and are porous. Micron and submicron powders—which are commonly prepared from condensation of metal vapors in inert gases, precipitation from metal salt solutions, or decomposition of metal hydrides/carbonyls—are generally spherical (Hausner and Mal, 1982; Figlarz et al., 1992). The current work only considers spherical cladding particles.

All metals except gold tend to form oxides when exposed to oxygen. For many metals, such as aluminum, copper, chromium, and nickel, the oxide layer formed at relatively low temperatures, e.g., 200°C, is compact and pore-free, which effectively prevents further oxidation (Hauffe, 1965). As a result, the oxide layer is very thin. For example, at room temperature the oxide layer on aluminum grows very fast in the first few minutes, and then stops growing after one month, attaining a thickness of 45 Å (Kubaschewski and Hopkins, 1953). Furthermore, during laser cladding, argon gas is often used to prevent the cladding powder and cladding surface from oxidation. Therefore, this study neglects the effects of the thin metal oxide layer on radiation absorption.

Drude's Free-Electron Theory. For infrared radiation, optical properties of metals and their temperature dependence can be modeled by Drude's free-electron theory (Ujihara, 1972; Arnold, 1984; Bruckner et al., 1991). In Drude's theory, free electrons in metals behave like a gas, which has remarkable mobility within the closely packed atoms, that determines fundamental optical and transport properties of metals. The complex refractive index of metals, $m = n + ik$, is characterized by the plasma frequency of electrons, ω_p, and the electron-lattice collision frequency, γ, as (Bohren and Huffman, 1983)

$$m = n + ik = \left[1 - \frac{\omega_p^2}{\omega(\omega + i\gamma)}\right]^{1/2} \quad (1)$$

where ω is the angular frequency of the incident radiation. The plasma frequency depends on temperature very weakly below the melting point, while the electron-lattice collision frequency is

Contributed by the Heat Transfer Division and presented at the AIAA/ASME Thermophysics and Heat Transfer Conference, Colorado Springs, Colorado, June 19–23, 1994. Manuscript received by the Heat Transfer Division September 1993; revision received May 1994. Keywords: Radiation, Radiation Interactions. Associate Technical Editor: M. F. Modest.

strongly temperature dependent, as indicated by its relationship with the direct-current resistivity, R, as (Kittel, 1986)

$$\gamma(T) = \frac{n_e e^2}{m_e} R(T) \tag{2}$$

where n_e is the free-electron number density, e the electron charge, and m_e the effective mass of electrons. In the temperature range from 300 K to 900 K, the electrical resistivity of aluminum, chromium, and nickel increases linearly with temperature (Lide, 1992). Therefore the collision frequency is also linearly dependent on temperature. The evaluated temperature coefficients for aluminum, chromium, and nickel, $\alpha = d\gamma/\gamma_0 dT$, along with γ_0 and ω_p are listed in Table 1, where γ_0 is the collision frequency at 300 K. The temperature dependence of the collision frequency gives rise to the temperature dependence of infrared optical properties of metals.

Electromagnetic Wave Theory. Laser interactions with particles can be described by classical electromagnetic wave theory. When the beam diameter is large compared to the particle diameter, the laser beam can be treated as a monochromatic plane wave. Figure 1 shows a spherical polar coordinate system for a particle irradiated by a laser beam traveling along the Z axis. The particle absorbs the incident radiation energy by Joule heating (Born and Wolf, 1989),

$$Q(r, \theta, \phi) = \tfrac{1}{2}\sigma |\mathbf{E}(r, \theta, \phi)|^2 \tag{3}$$

where Q is the local radiation absorption, σ the electrical conductivity of the particle at the incident radiation frequency, and $\mathbf{E}$ the local electric field strength. Equation (3) can be further expressed in terms of the incident radiation intensity, I_0, wavelength, λ, and refractive index, n and k, as (Tuntomo et al., 1991)

$$Q(r, \theta, \phi) = \frac{4\pi n k I_0}{\lambda} S(r, \theta, \phi) \tag{4}$$

$$S(r, \theta, \phi) = |\mathbf{E}(r, \theta, \phi)/E_0|^2 \tag{5}$$

where E_0 is the incident electric field strength, and S is the dimensionless distribution of radiation absorption. The electric field vector inside the particle can be obtained by solving the Maxwell equations. Its three components are (Bohren and Huffman, 1983)

$$E_r = \frac{E_0 \cos\phi}{m^2\rho^2} \sum_{n=1}^{\infty} i^{n-1}(2n+1) d_n \psi_n(m\rho) P_n^1(\cos\theta) \tag{6}$$

$$E_\theta = \frac{E_0 \cos\phi}{m\rho} \sum_{n=1}^{\infty} \frac{i^n(2n+1)}{n(n+1)} \times \left[c_n \psi_n(m\rho) \frac{P_n^1(\cos\theta)}{\sin\theta} - i d_n \psi_n'(m\rho) \frac{dP_n^1(\cos\theta)}{d\theta} \right] \tag{7}$$

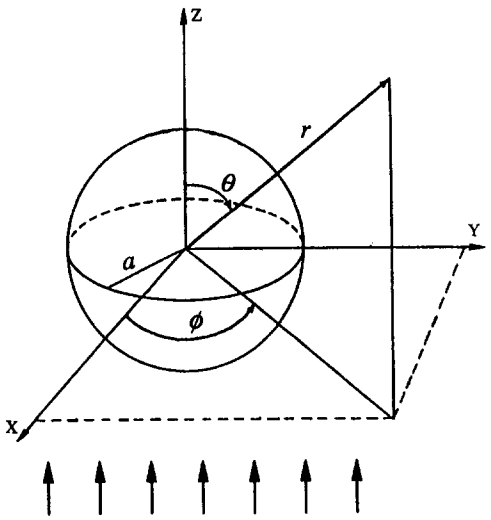

Fig. 1 Spherical polar coordinate system for an irradiated particle

$$E_\phi = \frac{E_0 \sin\phi}{m\rho} \sum_{n=1}^{\infty} \frac{i^{n+1}(2n+1)}{n(n+1)} \times \left[i c_n \psi_n(m\rho) \frac{dP_n^1(\cos\theta)}{d\theta} + d_n \psi_n'(m\rho) \frac{P_n^1(\cos\theta)}{\sin\theta} \right] \tag{8}$$

where ρ is the dimensionless radial coordinate given by

$$\rho = \frac{2\pi r}{\lambda} \tag{9}$$

The function ψ_n is the Riccati–Bessel function of order n, the prime denotes differentiation with respect to the argument, $P_n^1(\cos\theta)$ is the associated Legendre polynomial, and c_n and d_n are the expansion coefficients,

$$c_n = \frac{m\psi_n(x)\xi_n'(x) - m\psi_n'(x)\xi_n(x)}{\psi_n(mx)\xi_n'(x) - m\psi_n'(mx)\xi_n(x)} \tag{10}$$

$$d_n = \frac{m\psi_n(x)\xi_n'(x) - m\psi_n'(x)\xi_n(x)}{m\psi_n(mx)\xi_n'(x) - \psi_n'(mx)\xi_n(x)} \tag{11}$$

where $x = \pi d/\lambda$ is the size parameter and ξ_n is the Riccati–Bessel function of the third kind (Abramowitz and Stegun, 1970). For linearly polarized radiation, ϕ represents the angle between the polarization plane and the X–Z plane. For unpolarized or circularly polarized radiation, the internal field can be obtained by setting $\phi = \pi/4$ (Macowski, 1989).

The radiation absorptivity of the particle can be represented by the absorption cross section, C_a, which is the ratio of the total

Nomenclature

A = absorptivity of a flat surface
C_a = absorption cross section
d = particle diameter
$\mathbf{E}$ = electric field vector
i = $\sqrt{-1}$
I_0 = intensity of incidence radiation
k = imaginary part of refractive index
m = complex refractive index = $n + ik$
n = real part of refractive index
P = skin-depth parameter = $d/2\delta$
P_n^1 = associated Legendre polynomial
Q = distribution of radiation absorption
Q_a = absorption efficiency
Q_{av} = volumetric absorption efficiency
r = radial coordinate
R = electrical resistivity
S = normalized source function
T = temperature
x = size parameter = $\pi d/\lambda$
α = temperature coefficient of γ; $\alpha = d\gamma/\gamma dT$
γ = electron-lattice collision frequency
δ = skin depth = $\lambda/4\pi k$
θ = polar coordinate
λ = wavelength
ξ_n = Riccati–Bessel function of the third kind
ρ = dimensionless radial coordinate = $2\pi r/\lambda$
σ = electrical conductivity
ϕ = azimuthal coordinate
ψ_n = Riccati–Bessel function of the first kind
ω = angular frequency
ω_p = plasma frequency of free electrons

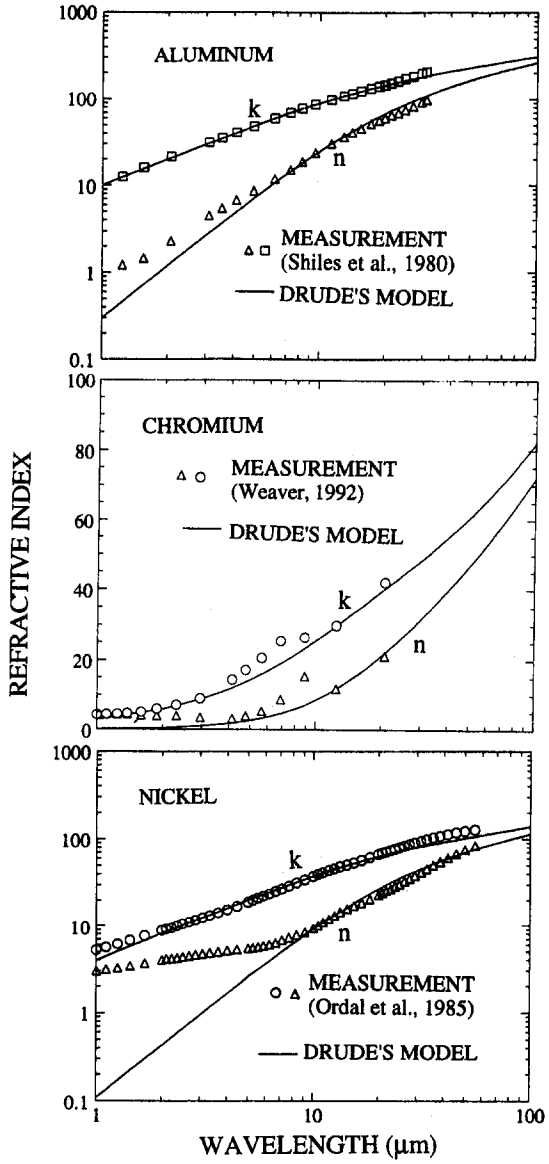

Fig. 2 Comparison between prediction and measurements

amount of absorbed energy to the incident radiation intensity. It can be evaluated either by integrating the absorbed radiation energy inside the particle or by subtracting the energy scattered by the particle from the total radiation extinction (Bohren and Huffman, 1983),

$$C_a = \frac{\lambda^2}{2\pi} \sum_{n=1}^{\infty} (2n+1)[\mathrm{Re}(a_n + b_n) - (|a_n|^2 + |b_n|^2)] \quad (12)$$

$$a_n = \frac{m\psi_n(mx)\psi_n'(x) - \psi_n(x)\psi_n'(mx)}{m\psi_n(mx)\xi_n'(x) - \psi_n'(mx)\xi_n(x)} \quad (13)$$

$$b_n = \frac{\psi_n(mx)\psi_n'(x) - m\psi_n(x)\psi_n'(mx)}{\psi_n(mx)\xi_n'(x) - m\psi_n'(mx)\xi_n(x)} \quad (14)$$

The efficiency for a particle to absorb radiation can be characterized by the *absorption efficiency* based on its cross-sectional area, $Q_a = C_a/(\pi d^2/4)$, and the *volumetric absorption efficiency* based on its volume, $Q_{av} = 6C_a/\pi d^3$.

Numerical Scheme. The optical properties were calculated from Eq. (1). The local radiation absorption and the total absorption in particles were obtained by solving Eqs. (4)–(8) and (12) numerically. The Riccati–Bessel function and its derivative in the expansion coefficients, a_n, b_n, c_n, and d_n, were computed from the Miev0 code (Wiscombe, 1979). The grid points in the r and θ direction are 50 and 180, respectively. Results calculated with doubled grid points were virtually identical. The numerical accuracy was further checked by comparing the total absorbed energy by a particle evaluated from the *external-field* Mie calculation (Bohren and Huffman, 1983), Eq. (12), with that from the *internal-field* integration (Tuntomo et al., 1991). In all cases the difference was less than 2 percent.

Results and Discussion

Figure 2 shows the comparison between predictions of Drude's free-electron theory and published measurement data for aluminum, chromium, and nickel in the wavelength range from 1 μm to 100 μm at 300 K. The parameters used in Drude's theory, ω_p and γ_0, are deduced by best fitting the experimental results in the wavelength region between 10 μm to 20 μm, and are listed in Table 1. For incident radiation with a relatively short wavelength, e.g., shorter than 5 μm, electrons experience relatively strong photon excitation and strong interactions with atoms. The electrons are not perfectly free, and thus predictions based on the free-electron assumption deviate from measured data. But for radiation with longer wavelengths, electrons behave like a free electron gas, and thus model predictions agree well with experimental data. The refractive index evaluated at 10.6 μm and 300 K for aluminum, chromium, and nickel is $27.3 + i93.8$, $9.4 + i26.7$, and $10.2 + i39.6$, respectively.

Figure 3 shows the local radiation absorption in nickel particles irradiated by an unpolarized CO_2 laser beam. The cross section of the particles lies in the $Y-Z$ plane, and the laser beam propagates along the Z axis. The local absorption pattern has distinctive features that depend on the dimensionless *particle size parameter* and the *skin-depth parameter*. The size parameter, $x = \pi d/\lambda$, characterizes the importance of the diffraction effect. The skin-depth parameter, which is defined as the ratio of the particle radius to the radiation skin depth of the particle ($\delta = \lambda/4\pi k$), $p = d/2\delta$, characterizes the radiation absorption inside the particle.

For large particles ($x \gg 1$), the effect of diffraction is small, and the incident radiation is absorbed mostly at the front particle surface. When x is of order one, diffraction becomes significant. The incident plane wave is bent around the particle surface, which in turn results in both front surface absorption and back surface absorption. In addition, the diffraction effect causes an oscillating pattern of radiation absorption around the particle surface. In the very small particle regime ($x \ll 1$), radiation absorption at the front and back surfaces approaches the same level. For large skin-depth parameters, the incident electromagnetic wave cannot penetrate deeply into the particle, thus radiation absorption is mainly a surface phenomenon. When the skin-depth parameter is comparable or smaller than one, the incident radiation can propagate inside the particle, resulting in more uniform internal radiation absorption.

Metals have extremely small skin depth, typically around 200 Å. As a result, the distribution of internal radiation absorption is still highly nonuniform for particles with a diameter as small as 0.5 μm ($x = 0.15$). This feature is very different from those in previous studies on radiation absorption in weakly absorbing particles (Tuntomo et al., 1991). In their case ($m = 1.5 + i0.1$),

Table 1 Drude's theory parameters

Parameters	Al	Cr	Ni
Plasma frequency, ω_p (s^{-1})	1.89×10^{16}	5.69×10^{15}	7.76×10^{15}
Collision frequency, γ_0 (s^{-1})	1.13×10^{14}	1.43×10^{14}	9.76×10^{13}
Temperature coefficient, α (K^{-1})	4.5×10^{-3}	3.5×10^{-3}	7.7×10^{-3}

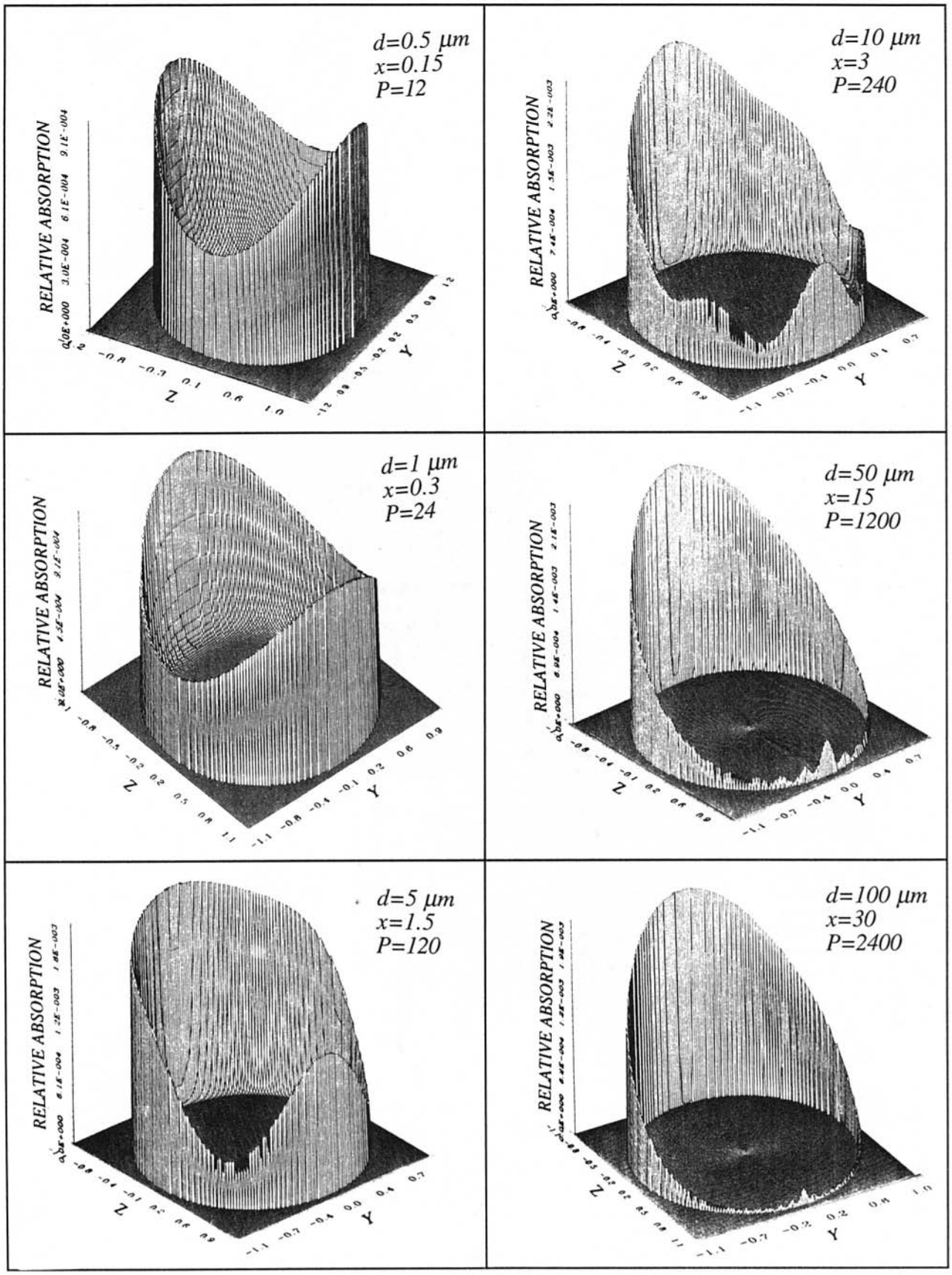

Fig. 3 Distributions of internal radiation absorption in nickel particles

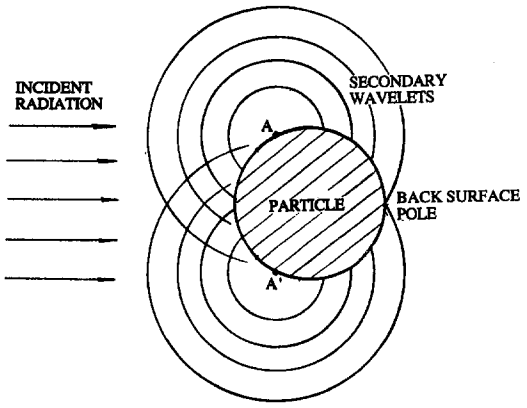

Fig. 4 Constructive interference of secondary wavelets at back surface pole

radiation absorption in particles becomes highly uniform for particle size parameters as large as $x = 0.5$.

An interesting phenomenon in the radiation absorption pattern is that the pole of the back particle surface always absorbs more radiation than its surrounding points, which is impossible under the geometric optics framework (Fig. 3). This phenomenon is due to the diffraction effect, which can be explained qualitatively by Huygens' principle (Fig. 4). Each element of a wave front can be regarded as the source of secondary spherical wavelets. The position of the wave front at a later time is the envelope of all such wavelets, and its intensity at a point results from interference of all the secondary wavelets at that point. For example, after the laser beam reaches the particle surface, each surface point starts to emit secondary wavelets. Due to the spherical symmetry, all surface points in a plane perpendicular to the incident beam emits secondary wavelets with the same intensity and phase, e.g., A and A' in Fig. 4. As the secondary wavelets from these points reach the back surface pole, they are all still in phase and thus form constructive interference. As a result, the back surface pole always receives the highest radiation relative to its neighboring points.

Figure 5 shows the volumetric absorption efficiency, Q_{av}, for aluminum, chromium, and nickel particles at 300 K and at the CO_2 laser wavelength. In the particle diameter region $d > 10$ μm, surface absorption dominates (Fig. 3). Therefore, Q_{av} decreases rapidly as the particle diameter increases. In the region 0.1 μm $< d < 10$ μm, Q_{av} has a maximum value for each metal, as a result of strong effects of light diffraction around the particle surface. Particles absorb radiation most efficiently in the region 0.1 μm $< d < 1$ μm. For vanishingly small particles (e.g., $d < 0.01$ μm), Q_{av}

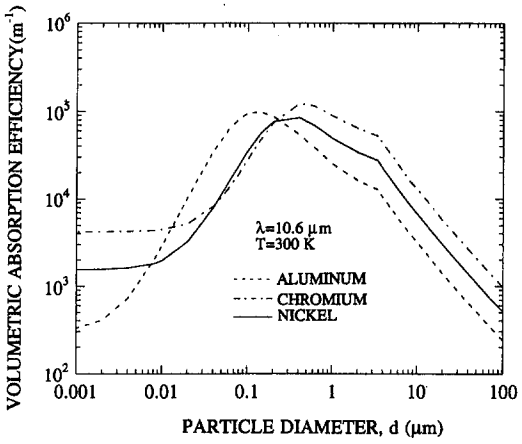

Fig. 5 Volumetric absorption efficiency at room temperature

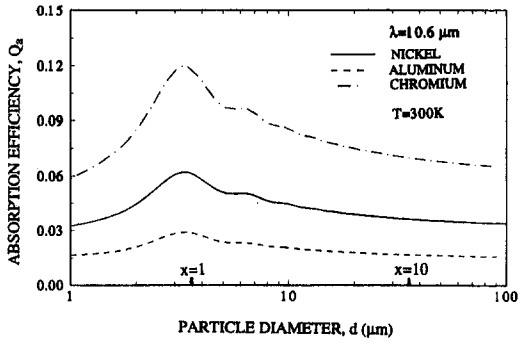

Fig. 6 Absorption efficiency based on cross-sectional area at room temperature

approaches a constant, which is the Rayleigh limit of light scattering by small particles (Bohren and Huffman, 1983),

$$Q_{av} = \frac{6\pi}{\lambda} \mathrm{Im}\left\{\frac{m^2 - 1}{m^2 + 2}\right\} \approx \frac{36\pi}{\lambda} \cdot \frac{nk}{(n^2 + k^2)^2} \qquad (15)$$

The Rayleigh region begins when particle diameters are comparable with the skin depth, which is 0.009 μm, 0.03 μm, and 0.02 μm for aluminum, chromium, and nickel, respectively. Therefore, metallic particles do not have the Rayleigh scattering behavior unless they are extremely small, e.g., approaching nanometers in diameters. For weakly absorbing particles, the Rayleigh solution provides an upper limit on Q_{av} (e.g., Tuntomo et al., 1991). For metallic particles, however, the maximum Q_{av} is about two orders of magnitude larger than the Rayleigh limiting value.

Figure 6 presents the cross-sectional area based particle absorption efficiency, Q_a, at room temperature. The absorption efficiency is very sensitive to the particle diameter for small par-

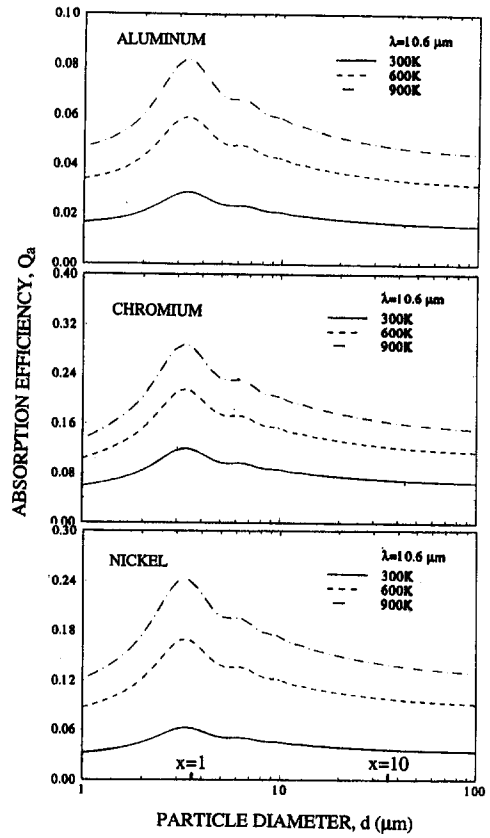

Fig. 7 Absorption efficiency at different temperatures

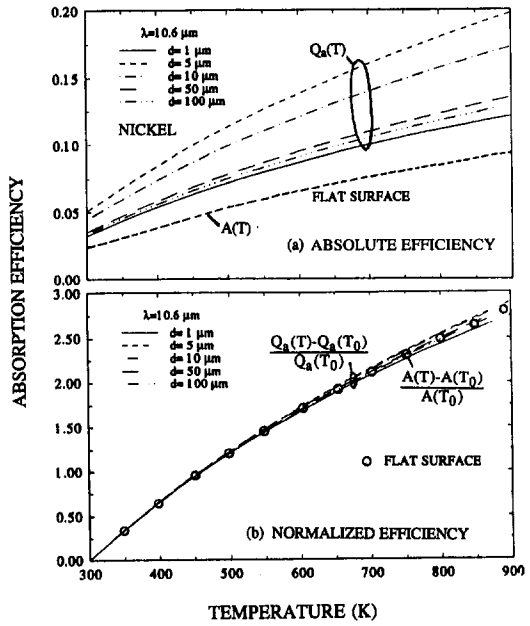

Fig. 8 Temperature dependence of radiation absorption for particles and flat surfaces

ticles and insensitive to the diameter for large particles. For size parameters around one, the absorption on the cross-sectional basis is most efficient due to the strong diffraction effect.

Figure 7 shows the absorption efficiency, Q_a, at 300 K, 600 K, and 900 K. The absorption efficiency increases with temperature uniformly for particles with diameters ranging from 1 μm to 100 μm. As the particle temperature increases from 300 K to 900 K, the absorption coefficient increases by about four, three, and two times, for nickel, aluminum, and chromium particles, respectively. Therefore, preheating of particles can effectively enhance radiation absorption in metallic particles.

Figure 8 shows the temperature dependence of radiation absorption for particles and flat surfaces. The normal-incident absorptivity of a flat surface is evaluated from the equation (Bohren and Huffman, 1983),

$$A(T) = \frac{4n}{(n+1)^2 + k^2} \tag{16}$$

The comparison between $Q_a(T)$ and $A(T)$ reveals two important features. First, due to the diffraction effect at the particle surface, particles can absorb more radiation energy than a flat surface with the same cross-sectional area. Second, spherical particles have the same temperature dependence of radiation absorption as a flat surface does at the normal incidence. Therefore, the effect of heating on the changes of Q_a can be simply estimated as

$$\frac{Q_a(T) - Q_a(T_0)}{Q_a(T_0)} \approx \frac{A(T) - A(T_0)}{A(T_0)} \tag{17}$$

where T_0 is a reference temperature.

Conclusions

The present work has applied the Drude free-electron theory and electromagnetic wave theory to characterizing internal absorption of CO_2 laser radiation in aluminum, chromium, and nickel powders. The results show that for large particles radiation absorption occurs only in a very narrow region of the front particle surface, which results in inefficient radiation absorption. On the other hand, for micron and submicron particles, the strong diffraction effect can bend the incident radiation around the particle surface, which in turn leads to very efficient radiation absorption on a volumetric basis compared to both large particles and vanishingly small particles. Furthermore, increasing the particle temperature from 300 K to 900 K can enhance radiation absorption in nickel, aluminum, and chromium particles by about four, three and two times, respectively. The particles have the same temperature dependence of radiation absorption as flat surfaces at the normal incidence.

Acknowledgments

The authors acknowledge the financial support from the U.S. National Science Foundation, the U.S. Department of Energy, and the K. C. Wang Education Foundation in Hong Kong.

References

Abramowitz, M., and Stegun, I. A., 1970, *Handbook of Mathematical Functions*, Dover, New York.

Arnold, G. S., 1984, "Absorptivity of Several Metals at 10.6 μm: Empirical Expressions for the Temperature Dependence Computed From Drude's Theory," *Applied Optics*, Vol. 23, pp. 1434–1436.

Atamert, S., and Bhadeshia, H. K. D. H., 1989, "Comparison of the Microstructures and Abrasive Wear Properties of Stellite Hardfacing Alloys Deposited by Arc Welding and Laser Cladding," *Metallurgical Transactions A*, Vol. 20, pp. 1037–1054.

Avner, A. H., 1964, *Introduction to Physical Metallurgy*, McGraw-Hill, New York.

Bohren, C. F., and Huffman, D. R., 1983, *Absorption and Scattering of Light by Small Particles*, Wiley, New York.

Born, M., and Wolf, E., 1989, *Principles of Optics*, 6th ed., Pergamon Press, New York.

Brewster, M. Q., 1992, *Thermal Radiative Transfer and Properties*, Wiley, New York.

Brewster, M. Q., and Tien, C. L., 1982, "Radiative Transfer in Packed and Fluidized Beds: Dependent vs. Independent Scattering," ASME JOURNAL OF HEAT TRANSFER, Vol. 104, pp. 573–579.

Bruckner, M., Schafer, J. H., Schiffer, C., and Uhlenbusch, J., 1991, "Measurements of the Optical Constants of Solid and Molten Gold and Tin at $\lambda = 10.6$ μm," *J. Applied Physics*, Vol. 70, pp. 1642–1647.

Figlarz, M., Ducamp-Sanguesa, C., Fievet, F., and Lagier, J-P., 1992, "Preparation and Characterization of Monodisperse Co, Ni, Cu, and Ag Metal Particles of Uniform Shape," in: *Advances in Powder Metallurgy and Particulate Materials*, Vol. 1, J. M. Capus and R. M. German, eds., American Powder Metallurgy Institute, Princeton, NJ.

Hauffe, K., 1965, *Oxidation of Metals*, Plenum Press, New York.

Hausner, H. H., and Mal, M. K., 1982, *Handbook of Powder Metallurgy*, Chemical Publishing Co., New York.

Hoadley, A. F. A., and Rappaz, M., 1992, "A Thermal Model of Laser Cladding by Powder Injection," *Metallurgical Transactions B*, Vol. 23, pp. 631–642.

Kittel, C., 1986, *Introduction to Solid State Physics*, 6th ed., Wiley, New York.

Komvopoulos, K., and Nagarathnam, K., 1990, "Processing and Characterization of Laser-Cladded Coating Materials," ASME *Journal of Engineering Materials and Technology*, Vol. 112, pp. 131–143.

Kubaschewski, O., and Hopkins, B. E., 1953, *Oxidation of Metals and Alloys*, Academic Press, New York.

Lide, D. R., ed., 1992, *CRC Handbook of Chemistry and Physics*, 73rd ed., CRC Press, Boca Raton, FL, Section 12, pp. 34–35.

Mackowski, D. W., 1989, "Photophoresis of Aerosol Particles in the Free Molecular and Slip-Flow Regimes," *Int. J. Heat Mass Transfer*, Vol. 32, pp. 843–854.

Mazumder, J., Sircar, S., Ribaudo, C., and Kar, A., 1992, "Laser Cladding of Nonequilibrium Metallic Alloys," in: *Thermomechanical Aspects of Manufacturing and Materials Processing*, R. K. Shah et al., eds., Hemisphere Publishing Corp., New York, pp. 319–335.

Oberlander, B. C., and Lugscheider, E., 1992, "Comparison of Properties of Coatings Produced by Laser Cladding and Conventional Methods," *Materials Science and Technology*, Vol. 8, pp. 657–665.

Ordal, M. A., Bell, R. J., Alexander, R. W., Long, L. L., Jr., and Querry, M. R., 1985, "Optical Properties of Fourteen Metals in the Infrared and Far Infrared: Al, Co, Cu, Au, Fe, Pb, Mo, Ni, Pd, Pt, Ag, Ti, V, and W," *Applied Optics*, Vol. 24, pp. 4493–4499.

Prokhorov, A. M., and Konov, V. I., 1990, *Laser Heating of Metals*, Adam Hilger, New York.

Pustovalov, V. K., and Bobuchenko, D. S., 1993, "Thermal Processes in Gas-Powder Laser Cladding of Metal Materials," *Int. J. Heat Mass Transfer*, Vol. 36, pp. 2449–2456.

Shiles, E., Sasaki, T., Inokuti, M., and Smith, D. Y., 1980, "Self-Consistency and Sum-Rule Tests in the Kramers-Kroning Analysis of Optical Data: Applications to Aluminum," *Physical Review B*, Vol. 22, pp. 1612–1628.

Tuntomo, A., Tien, C. L., and Park, S. H., 1991, "Internal Distribution of Radiant Absorption in a Spherical Particle," ASME JOURNAL OF HEAT TRANSFER, Vol. 113, pp. 407–412.

Ujihara, K., 1972, "Reflectivity of Metals at High Temperatures," *J. Applied Physics*, Vol. 43, pp. 2376–2383.

Weaver, J. H., 1992, "Optical Properties of Metals," in: *CRC Handbook of Chemistry and Physics*, 73rd ed., D. R. Lide, ed., CRC Press, Boca Raton, FL, Section 12, pp. 111–126.

Wiscombe, W. J., 1979, "Mie Scattering Calculations: Advances in Technique and Fast, Vector-Speed Computer Codes," NCAR Technical Report #NCAR/TN-140+STR, NCAR, Boulder, CO.